β1-adrenergic receptor on pyramidal neurons of mPFC regulates METH-preferred behaviors in METH-sired male mice

Yanyan Zheng[1,2], Zhaosu Li[1,2], Jun Wen[1], Wenwen Chen[1], Hao Guo[1], Zhen Cheng[1], Tao Hu[1], Yuanyuan Zhang[1], Ziheng Zhao[1], Qinglong Cai[1], Feifei Ge[1], Yu Fan[1,*], Dekang Liu[1,*], Xiaowei Guan[1,*]

[1]Department of Human Anatomy and Histoembryology, Nanjing University of Chinese Medicine, Nanjing 210023, China

[2] These authors are equally contribute to this work

Running title: mPFC ADRB1 and CPP in METH-sired mice

*Correspondence to: Prof. Xiaowei Guan (guanxw918@njucm.edu.cn), Dr. Yu Fan (yfan@njucm.edu.cn), Dr. Dekang Liu (dekang@njucm.edu.cn)

Phone number: +86-15295560773

Abstract

As a highly addictive psychostimulant drug, paternal methamphetamine (METH) exposure enhances the risk of developing addiction to drugs in descendants, however the underlying mechanism remains unclear. Medial prefrontal cortex (mPFC) is a key brain region that implicated in susceptibility to drugs. Here, male adult mice were exposed to METH for 30 days, followed by mating with naïve female mice to create the first-generation (F1) mice. In METH-sired mice, baseline levels of c-Fos were decreased but β1-adrenergic receptor (ADRB1) were increased in mPFC by paternal METH exposure. Trained with subthreshold-dosed administration of METH, METH-sired mice exhibited significant METH-preferred behaviors, accompanied with higher levels of c-Fos, ADRB1 and dendritic spines density in mPFC. Importantly, local blocking ADRB1 activity or specific knockdown of ADRB1 on excitatory neurons of mPFC, both efficiently inhibited METH-preferred behaviors in METH-sired mice. In parallel, levels of p-ERK1/2 and ΔFosB, as well as dendritic spine density were reduced by knocking-down mPFC ADRB1 in METH-sired mice. Collectively, these findings suggested that targeting ADRB1 signals in mPFC may represent a promising therapeutic strategy for preventing drug addiction, particularly in progeny with a history of paternal drugs exposure.

Keywords: METH-sired offspring, METH-preferred behaviors, mPFC, β1-adrenergic receptor

Significance statement

METH-sired mice exhibit higher susceptibility to METH, accompanied with increased mPFC activity and ADRB1 levels in response to METH administration. Local blocking ADRB1 or specific knockdown of ADRB1 on excitatory neurons of mPFC efficiently block METH-preferred behaviors in METH-sired mice, of which p-ERK1/2 and ΔFosB are key downstream molecules of ADRB1 in the process.

Introduction

Methamphetamine (METH) is a highly addictive psychostimulant drug. Paternal abuse of psychostimulants increases the risk of developing addiction to drugs in descendants (1, 2), but the underlying mechanism remains unclear. One recent study found that METH-sired rats exhibited sensitized behaviors in response to acute drug use (3), indicating a higher susceptibility of offspring to drug addiction by paternal METH use. The medial prefrontal cortex (mPFC) has been considered as key brain regions implicated in the processes of reward (4, 5), METH addiction (6, 7) and susceptibility to drugs of abuse (8-10). Human imaging studies showed a significantly affected the volume, cortical thickness and connection, especially that of the prefrontal cortex (PFC) (9, 11, 12) in brains of offspring who exposed to METH prenatally. Previously, we found that activities of mPFC were blunted to gentle stressor in METH-sired first-generation (F1) mice, indicating an important role of mPFC in the neurotoxic effects of paternal METH on offspring. However, the intrinsic molecular mechanisms of mPFC underlying the paternal METH exposure-promoted susceptibility of offspring to drugs remain largely unknown.

Adrenergic innervation of mPFC pyramidal neurons plays an essential role in both physiology (attention, working memory, and cognitive behavior) and pathophysiology (addiction, attention deficit hyperactivity disorder, posttraumatic stress disorder, and depression). β1-adrenergic receptor (ADRB1) are critically involved in cognition (13, 14), reward (15) , arousal (16), motivation (17), and stress-related behaviors (18). In mPFC, specific activation of ADRB1 triggers the excitability of PFC neurons (19). Further, high dose of ADRB1 efficiently block stress-induced cocaine reinstatement in animals (20). Prenatal events exposure, malnutrition for example, impairs the long-term potentiation in PFC and memory performance in offspring (21-23), which could be fully

recovered by ADRB1 activation, indicating important role of ADRB1 in processes of intergenerational or transgenerational neurotoxicity by prenatal harmful experiences. Yet, the role of mPFC ADRB1 in susceptibility to drugs in METH-sired progeny remains unclear.

As one of classical G protein coupled receptors (GPCRs), ADRB1 has been well-studied to be coupled to Gs protein which lead to an increase in protein kinase A (PKA)-dependent signaling pathway including cAMP, PKA, and cAMP response element-binding protein (CREB) (13, 24). Recently, it has become evident that β-arrestin2-dependent β-adrenergic signaling pathway is required in excitatory neurons of PFC for extinction learning of cocaine-induced conditioned place preference (CPP) (25).

In the present study, male adult mice were exposed to METH for 30 days, followed by mating with naïve female mice to create the first-generation (F1) mice. When the F1 mice growing up to early adult age, a subset of male F1 offspring were subjected to METH-induced CPP behaviors to evaluate their susceptibility to drugs addiction, and the other male F1 mice were to explore the role of mPFC ADRB1 in the development of METH-elicited preference behaviors.

Results

METH-sired mice exhibited METH-preferred behaviors

To assess susceptibility of METH-sired mice to drugs, subthreshold doses of METH (0.25 mg /kg) was used to induce CPP behaviors in male F1 mice (Figure 1a). As shown in Figure 1b-d, subthreshold dose of METH failed to induce CPP behaviors in SAL-sired mice (n = 8, $t = 0.9474$, $P = 0.5872$, Figure 1b), but increased CPP score of METH-sired mice (n = 10, $t = 6.587$, $P < 0.0001$, Figure 1b) when compared with their Pre-test

data. The ΔCPP score (n = 18, t = 3.685, P = 0.002, Figure 1c) in METH-sired mice was higher than that in SAL-sired mice.

The neuronal activity and ADRB1 in mPFC were at higher levels in response to METH administration in METH-sired mice

The mPFC tissue were collected from F1 mice on PD60 and PD73, which represent the baseline condition and responsive condition to METH injection, respectively. The c-Fos, CaMKII and NeuN are used as markers to assess mPFC activities, labeling excitatory (pyramidal) neurons and total neurons in the morphological experiments, respectively. On PD60, there was no significance in the percentage of c-Fos-positive pyramidal neurons (labeled as CaMKII-positive neurons) in subregions of mPFC including cingulate cortex (Cg1, n = 6, t = 0.595, P = 0.5839), prelimbic cortex (PrL, n = 6, t = 0.0371, P = 0.9722) and infralimbic cortex (IL, n = 6, t = 0.4451, P = 0.6793) between METH-sired and SAL-sired mice (Figure 1e). While on PD73, after METH-induced CPP, the percentage of c-Fos-positive pyramidal neurons were at higher levels in Cg1 (n = 8, t = 3.447, P = 0.0137), PrL (n = 10, t = 3.539, P = 0.0076) and IL (n = 10, t = 3.160, P = 0.0134) in METH-sired mice than that in SAL-sired mice (Figure 1f). On PD73, the neurons (labeled as NeuN-positive neurons) were more activated in Cg1 (n = 10, t = 3.031, P = 0.0163), PrL (n = 11, t = 4.227, P = 0.0022) and IL (n = 11, t = 4.098, P = 0.0027, Figure S1a), and the dendritic spine density of mPFC pyramidal neurons was increased (n = 8, t = 4.960, P = 0.0026, Figure S1b) in METH-sired mice, when compared with SAL-sired mice. As one of important kinase, CaMKII can also be used to reflect the activities of neurons. On PD60, the baseline levels of mPFC c-Fos (n = 12, t = 3.496, P = 0.0058) and CaMKII protein (n = 12, t = 2.457, P = 0.0338) were obviously lower in METH-sired mice than that in SAL-sired mice (Figure 1g). On PD73, after METH-induced CPP, there was similar levels of c-Fos protein (n = 12, t =

0.5061, P = 0.6238) but a higher levels of CaMKII protein (n = 12, t = 3.350, P = 0.0074) in METH-sired mice compared to SAL-sired mice (Figure 1h).

In parallel, the baseline levels of mPFC *Adrb1* mRNA (n = 6, t = 3.084, P = 0.0368, Figure 1i) and ADRB1 protein (n = 12, t = 2.400, P = 0.0373, Figure 1j) were higher in METH-sired mice than that in SAL-sired mice on PD60. After METH exposure, mPFC *Adrb1* mRNA (n = 6, t = 4.621, P = 0.0099, Figure 1i) and ADRB1 protein (n = 7, t = 3.489, P = 0.0175, Figure 1j) were persistently at higher levels in METH-sired mice on PD73, when compared with that in SAL-sired mice. The ADRB1 expressions in mPFC neurons were examined by immunostaining. As shown Figure 1k, the mean gray value of ADRB1 in mPFC neurons was much higher in the Cg1 (n = 6, t = 4.649, P = 0.0097) and PrL (n = 6, t = 4.311, P = 0.0125), but a high trend in IL (n = 6, t = 2.265, P = 0.0862) of METH-sired mice, when compared to that in SAL-sired mice on PD60. After METH-induced CPP, the mean gray value of ADRB1 in mPFC neurons was much higher in PrL (n = 6, t = 6.304, P = 0.0032), but a higher trend in Cg1 (n = 6, t = 2.382, P = 0.0758) and IL (n = 6, t = 2.635, P = 0.0579) of METH-sired mice, when compared to that in SAL-sired mice on PD73 (Figure 1l).

To observe the effects of subthreshold-dosed METH on levels of c-Fos and ADRB1 in mPFC, male naïve mice were subjected to subthreshold doses of METH treatment (Figure S2a). As shown in Figure S2b, the mRNA levels of *c-Fos* (n = 6, t = 0.4522, P = 0.6745) and *Adrb1* (n = 6, t = 0.9778, P = 0.3835) were not changed by subthreshold-dosed METH exposure in mPFC of naïve mice. Similarly, the protein levels of c-Fos (n = 6, t = 1.115, P = 0.3274) and ADRB1 (n = 6, t = 1.723, P = 0.1600) were not changed by METH exposure in mPFC (Figure S2c).

Specific blockade of ADRB1 in mPFC suppressed METH-induced CPP behaviors

in METH-sired mice

To evaluate the role of ADRB1 in the METH-induced CPP behaviors in METH-sired mice, betaxolol was bilaterally injected into mPFC during CPP training or prior to CPP test (Figure S3a). In Experiment 1, METH-sired mice with a single dose of local betaxolol administration at 15 min prior to CPP test failed to exhibit METH-preferred behavior (n = 8, t = 1.666, P = 0.2219), but METH-sired mice with vehicle treatment exhibited CPP behavior (n = 8, t = 3.518, P = 0.0068). The ΔCPP score (n = 16, t = 3.666, P = 0.0025) in vehicle-injected METH-sired mice was much higher than that in betaxolol-injected METH-sired mice (Figure 2a-d). In Experiment 2, local betaxolol injection during CPP training inhibit METH-induced CPP behavior in METH-sired mice (n = 8, t = 0.2852, P = 0.9514), and vehicle injection failed to affect METH-induced CPP behavior in METH-sired mice (n = 8, t = 6.570, P < 0.0001). The ΔCPP score (n = 16, t = 4.847, P = 0.0003) in vehicle-injected METH-sired mice was much higher than that in betaxolol-injected METH-sired mice (Figure 2e-h).

Specific knockdown of ADRB1 in pyramidal neurons of mPFC blocked METH-induced CPP behaviors in METH-sired mice

Specific knockdown of ADRB1 expression in pyramidal neurons of mPFC were performed to further examine the role of ADRB1 in METH-induced CPP behaviors (Figure 3a). As shown in Figure 3b, adeno-associated virus of *CaMKIIap-EGFP-MIR155(MCS)-SV40PolyA* (KD group) and *CaMKIIap-EGFP-SV40PolyA* (Ctrl group) were bilaterally infused into mPFC, as well as about 80% neurons (Figure S4a) and above 60% pyramidal neurons (labeled as CaMKII-positive neurons, Figure 3c) within mPFC were transfected with virus. As shown in Figure 3d-f, the mRNA (n = 6, t = 7.361, P = 0.0018), protein (n = 6, t = 3.418, P = 0.0268) and mean gray value (n = 6,

t = 4.237, P = 0.0133) of ADRB1 were reduced in mPFC of METH-sired mice by KD virus, when compared with Ctrl virus.

As shown Figure 3g-i, METH-sired mice with selective knockdown of ADRB1 in mPFC exhibited no METH-preferred behaviors which even produced METH-aversion behaviors (n = 10, t = 3.253, P = 0.008), while Ctrl virus treatment failed to affect METH-induced CPP in METH-sired mice (n = 12, t = 8.228, P < 0.0001), when compared with their corresponding baseline score (Pre-test). The ΔCPP score of METH-sired mice in KD group was lower than that in Ctrl group (n = 22, t = 7.95, P < 0.0001).

Specific knockdown of ADRB1 in pyramidal neurons of mPFC partially attenuated neuronal excitatory responses to METH in METH-sired mice

As shown in Figure 4a-b, the c-Fos immunostaining (n = 7, t = 2.767, P = 0.0395) and protein levels (n = 6, t = 5.372, P = 0.0058) were decreased, while CaMKII levels were increased (n = 6, t = 4.850, P = 0.0083) in mPFC by ADRB1 knockdown in METH-sired mice compared to Ctrl virus group, indicating the c-Fos-dependent but not CaMKII-dependent neuron excitability is associated with mPFC ADRB1 in METH-sired mice. In parallel, the dendritic spine density of pyramidal neurons in mPFC were reduced by knockdown of ADRB1 in METH-sired mice (n = 12, t = 3.891, P = 0.003, Figure 4c).

Some downstream molecules of ADRB1 were downregulated by ADRB1 knockdown in METH-sired mice

To determine the involvement of potential molecules of β-adrenergic signaling pathways in METH-sired mice, the molecules related to ADRB1, especially β-arrestin2 and PKA, were examined in the present study. As shown in Figure 4d, the levels of two

core proteins of β-adrenergic signaling pathways, including β-arrestin2 (n = 12, t = 0.4597, P = 0.6555) and PKA (n = 6, t = 0.6055, P = 0.5775) were not changed by ADRB1 knockdown, when compared to Ctrl virus group. While, as shown in Figure 4e, the p-ERK1/2 (n = 11, t = 8.202, P < 0.0001), ratio of p-ERK1/2 to ERK1/2 (n = 11, t = 2.486, P = 0.0347) and ΔFosB (n = 12, t = 2.944, P = 0.0147) were decreased, but ERK1/2 (n = 11, t = 0.9153, P = 0.3839), CREB (n = 6, t = 0.5454, P = 0.6145), p-CREB (n = 6, t = 0.8085, P = 0.4641) and ratio of p-CREB to CREB (n = 6, t = 0.6042, P = 0.5783) were not changed by ADRB1 knockdown, when compared to Ctrl virus group.

Discussion

The current study found that paternal METH exposure attenuated the baseline of neuronal activities, but increased ADRB1 level in mPFC of METH-sired male mice. In response to subthreshold-dosed administration of METH, METH-sired mice exhibited METH-preferred behaviors, accompanied with more triggered neuronal activities and dendritic spines in glutamatergic neurons of mPFC. Importantly, local blockade of ADRB1 or specific knockdown of ADRB1 on glutamatergic neurons of mPFC, both efficiently inhibited the METH-preferred behaviors in METH-sired mice. In parallel, neuronal activities, dendritic spine density, protein levels of p-EKR1/2 and ΔFosB in mPFC were attenuated by ADRB1 knockdown in METH-sired mice (Figure 5).

METH is commonly abused illicit drugs among men of reproductive age. Emerging evidences have found that paternal drugs exposure heightened the risk of susceptibility to drugs in the subsequent generations (26-29). Consistent with previous studies, we found that subthreshold doses of METH effectively induced METH-preferred behaviors in METH-sired male mice, indicating an enhanced sensitivities to drugs in F1 mice paternally exposed to METH. The mPFC has been implicated in the

vulnerability to drug abuse (8-10). Currently, little literature has reported the association of paternal METH exposure with mPFC alteration in offspring, only some studies focusing effects of prenatal cocaine exposure on mPFC. *In utero* exposure to cocaine had been reported to increase the induction of long-term potentiation (LTP) and neuronal excitability at pyramidal neurons in mPFC of offspring (30), an increase in dendritic spines of II/III layer of pyramidal neurons in mPFC of offspring (31) , and a reduction of the sensitivity of locomotor activity to cocaine in prenatally cocaine exposed-rats (30, 32). By contrast, Yan et al. (33) reported prenatal cocaine exposure attenuated baseline levels of mature BDNF protein in the offspring, and Cantacorps et al. (34) found prenatal alcohol exposure increased vulnerability to cocaine addiction in adult mice via a greater glutamate receptor in mPFC. Similarly, human imaging studies demonstrated that prenatal cocaine exposed-adolescents exhibited less capability of increasing their PFC activation in response to memory load (35), and infants with prenatal cocaine use had a lesser gray matter in prefrontal brain regions (36, 37). In addition, adolescents with prenatal cocaine exposure had reduced activity in PFC when exposing to favorite-food cues (38). Although there are conflicting results among these studies, they suggest that PFC is implicated in susceptibility to drugs in offspring prenatally exposed to drugs. Here, we found that paternal METH exposure seemed to reduce the baseline of mPFC activities, especially of the excitatory neurons, in METH-sired mice, as indicated by lower levels of c-Fos and CaMKII in their mPFC. However, subthreshold doses of METH, which could not activate mPFC in naïve mice, reversely triggered more mPFC activities in METH-sired mice, indicating that paternal METH exposure potentiated the sensitivity of mPFC to METH in offspring.

ADRB1 is highly expressed on pyramidal neurons of mPFC. In general, endogenous activation of the β1 adrenergic receptor triggers neuronal excitabilities of mPFC via

eliciting the depolarization on the membrane potential in mPFC (39). An early study found that prenatal exposure to cocaine increased the cortical ADRB1 about 68% in their pup rats at 30 days of age, a time when these rats showed hyperactivity (40). Unfortunately, few studies further explored the role of this increase of cortical ADRB1 in prenatal cocaine-caused addiction or related psychiatric disorders. Administration of betaxolol, a selective ADRB1 antagonist, blocked stress-induced reinstatement of cocaine-induced CPP (20). Further, blockade of ADRB1 after cocaine retrieval impaired reconsolidation and reinstatement of cocaine self-administration (41). In this study, we found that the baseline levels of ADRB1 were higher on PD60. We believe that this higher baseline level of ADRB1 is kind of compensatory effect on paternal METH exposure-caused brain injury in offspring, which could strengthen the sensitivity of neurons to internal or external stimuli. To confirm this finding, by blocking mPFC ADRB1 or specific knockdown of ADRB1 on mPFC excitatory neurons, the METH-preferred behaviors were efficiently suppressed in METH-sired mice, indicating that the higher baseline levels of mPFC ADRB1 contribute to the higher sensitivity of mPFC to the stimulants including drugs, which ultimately enhances the susceptibility to drugs in METH-sired offspring.

ADRB1 activates neuronal excitability by regulating its downstream protein kinases and signal pathways (e.g. PKA, β-arrestin2), or mediating the function of nearby channels (e.g. TREK-2-like channels) or receptors (e.g. GluR1) on the membrane of cells. The critical role of ADRB1/cyclic-AMP dependent PKA in synaptic plasticity of the frontal cortex are well-studied (42). Recently, Huang et al. found that ADRB1/β-arrestin/ERK signaling in entorhinal cortex, acting as a non-classical G protein-coupled pathway, mediated memory reconsolidation (25). Their lab later reported that overexpression of β-arrestin2 in PFC promoted extinction learning of cocaine-induced

CPP, which was blocked by propranolol, a nonbiased β-adrenergic receptor antagonist (43). Thus, we detected the molecules related to ADRB1, especially those of β-arrestin2-dependent and PKA-dependent signal proteins. Unexpected, the levels of key proteins that are believed most importantly in β-adrenergic signaling pathway, including β-arrestin2 and PKA failed to change in mPFC after ADRB1 knockdown. While, we found that knockdown of ADRB1 could effectively reduce the levels of p-ERK1/2 and ΔFosB in mPFC. Son et al. (44) has been reported that acupuncture exert its therapeutic effects on METH-induced addiction via suppression of METH-increased p-ERK1/2 and ΔFosB in PFC. The p-ERK1/2 signaling cascades in PFC has been thought of important contributor for the development of METH addiction (45). ΔFosB, a transcription factor, is increased in PFC by drugs including METH (44) and Δ9-tetrahydrocannabinol (THC) (46), which leads to a long-lasting enhanced behavioral response. Further, ΔFosB is preferentially induced by cocaine in adolescent animals, which engaged in the higher vulnerability to addiction (47). Unlike c-Fos, Arc and ERK, ΔFosB maintains adaptive changes in brain for a long time following drugs of abuse (48). It is generally believed that ΔFosB is involved in the long-term pathological plasticity of brain and persistent addictive behavior by drugs (49). Collectively, these findings revealed that p-ERK1/2 and ΔFosB may be key downstream factors of ADRB1 that contribute to the higher suscepatibility of METH-sired mice to drug addiction. It is worth noting that the downstream molecules of ADRB1 interact with one another, which cannot be absolutely explained separately.

In conclusion, our findings suggested that ADRB1 in mPFC, especially on excitatory neurons, be essential regulator to mediate higher susceptibility to drug addiction in progeny paternally exposed to METH. Future studies are required to explore the genetic or epigenetic mechanisms by which paternal METH exposure alter the baseline levels

of ADRB1 in mPFC of offspring, and to find out the specific β-adrenergic signaling cascades in susceptibility to drugs of abuse in METH-sired offspring.

Materials and methods

Animals

Male C57BL/6 wild type (WT) mice weighing 22-25 g were used. All animals were housed at constant humidity (40~60%) and temperature (24 ± 2 ℃) with a 12-hour light/dark cycle and allowed free access to food and water. The animals were handled for three days prior to onset of experiments. All procedures were carried out in accordance with the National Institutes of Health Guide for the Care and Use of Laboratory Animals of China and approved by the Institutional Animal Care and Use Committee (IACUC) at Nanjing University of Chinese Medicine.

Drug treatment and tissue collection

Male C57BL/6 WT mice were assigned to administration of METH (5 mg/kg, dissolved in saline, i.p.) or saline (0.2 mL, i.p.) once daily at 10 a.m. for 30 consecutive days. At 24 hours after the last injection, the F0 mice were mated with three naïve female C57BL/6 WT mice for 4 days to create METH-sired or saline-sired first-generation (F1) offspring mice.

On postnatal day 21 (PD21), male F1 mice were weaned and kept (4 male mice in one cage) in homecages. On PD60, the mPFC tissue were collected from some male F1 mice. From PD70, some male F1 mice were subjected to METH-induced conditioned place preference (CPP) training and test. In this study, to examine the sensitivity to METH, subthreshold dose of METH (0.25 mg/kg) were used to induce CPP behavior in male F1 mice. Betaxolol, a specific β1-adrenergic receptor (ADRB1) antagonist (Cat# S2091, Sellekchem, USA) was diluted to 0.6 μg/μl in sterile saline. Brains of

male F1 mice were collected on PD60 and PD73. The brains of PD60 mice were collected without any treatment to represent baseline condition. The brains of PD73 mice were collected within 60 min after CPP test.

Some male naïve mice were only subjected to saline or METH treatment. On Day 1 (D1) and D2, mice were injected with saline (0.2 mL, i.p.) in the morning, and saline (0.2 mL, i.p.) or METH (0.25 mg/kg, i.p.) in the afternoon once daily (Figure S2a) at homecage. Their mPFC tissue were collected on D3 within 60 min of the last injection.

CPP

On PD70, some male F1 mice were subjected to METH-induced CPP behavioral tests. The CPP test was performed in the TopScan3D CPP apparatus (CleverSys, VA, USA), which is constructed of two distinct chambers (15 × 15 × 23 cm each) separated by a removable guillotine door. The CPP procedure consisted of three phases including the pre-conditioning test (Pre-test, PD70), conditioning (CPP training, PD71-72) and post-conditioning test (CPP test, PD73). During CPP training, both METH-sired and SAL-sired mice were injected with saline (0.2 mL, i.p.) in the morning or METH (0.25 mg/kg, i.p.) in the afternoon once daily. After each injection, the mice were confined to one conditioning chamber (SAL-paired chamber or METH-paired chamber) for 45 min, and then returned to their homecages. During the Pre-test and Test, mice freely access two chambers for 15 min. The CPP score is the time spent in METH-paired chamber minus that in SAL-paired chamber, and the ΔCPP score is the CPP score of Test minus the CPP score of Pre-test.

Immunofluorescence

Briefly, the brains were perfused with 4% paraformaldehyde (PFA), and coronal brain sections (30 μm) were cut on a cryostat (Leica, Germany). The sections were incubated

in 0.3% (v/v) Triton X-100 for 0.5 h, blocked with 5% donkey serum for 1.5 h at room temperature, and incubated overnight at 4℃ with the following primary antibodies: rabbit anti-c-Fos (1:3000, RRID:AB_2247211, Cell Signaling Technology, USA), mouse anti-NeuN (1:800, RRID:AB_2313673, Millipore, USA), mouse anti-CaMKII α (1:100, RRID:AB_626789, Santa Cruz Biotechnology, USA), Rabbit anti-ADRB1 (1:100, RRID:AB_10885544, Bioss, China), followed by the corresponding fluorophore-conjugated secondary antibodies for 1.5 h at room temperature. The following secondary antibodies were used here, including Alexa Fluor 555-labeled donkey anti-rabbit secondary antibody (1:500, RRID: AB_2762834, Thermo Fisher Scientific, USA), Alexa Fluor 488-labeled donkey anti-mouse secondary antibody (1:500, RRID: AB_141607, Thermo Fisher Scientific, USA). Fluorescence signals were visualized using a Leica DM6B upright digital research microscope (Leica, Germany) and Leica TCS SP8 confocal microscope (Leica, Germany).

Western blot

Total protein was extracted from mPFC of individual mouse using RIPA lysis buffer (Beijing ComWin Biotech Co., China), Phosphatase Inhibitor (Beijing ComWin Biotech Co., China), and Protease Inhibitor (Beijing ComWin Biotech Co., China) according to the manufacturer's instructions. Protein samples (15 or 20 μg) was separated by 10% SDS–PAGE, 12% SDS–PAGE and electrophoretically transferred onto PVDF membranes. The transferred membranes were blocked with 5% non-fat dry milk and 0.1% Tween 20 in TBST buffer for 2 h at room temperature, then subsequently incubated with the following primary antibodies: Rabbit anti-c-Fos (1:1000, RRID:AB_224721, Cell Signaling Technology, USA), Rabbit anti-GAPDH (1:10000, RRID:AB_2651132, Bioworld Technology, USA), Rabbit anti-CaMKII α (1:1000, RRID:AB_305050, Abcam, USA), Rabbit anti-ADRB1 (1:1000, RRID:AB_10885544,

Bioss, China), Mouse anti-β-actin (1:1000, RRID:AB_2687938, Proteintech, USA), Rabbit anti-ARRB2 (1:1000, BA3767, Boster, China), Rabbit anti-ERK1/2 (1:1000, BM4326, Boster, China), Rabbit anti-phospho-ERK1/2 (1:1000, BM4156, Boster, China), Rabbit anti-ΔFosB (1:1000, bsm-52071R, Bioss, China) , Rabbit anti-PKA (1:1000, bs-0520R, Bioss, China), Rabbit anti-CREB (1:1000, RRID:AB_2800317, Cell Signaling Technology, USA), Rabbit anti-phospho-CREB (1:1000, RRID:AB_2561044, Cell Signaling Technology, USA). The next day, the membranes were washed in Tris-buffered saline with Tween 20 (TBST) and incubated with horseradish peroxidase (HRP)-conjugated secondary antibody goat anti-rabbit or goat anti mouse (1:5000, Beijing ComWin Biotech Co., China) at room temperature for 1 h. The blots were visualized by the eECL Western Blot kit (Beijing ComWin Biotech Co., China, CW0049S) or ELC Kit (Vazyme^{TM}) and the signal was visualized by imaging system (Tanon-5200, Shanghai, China). The blots were washed with stripping buffer (Beyotime Institute of Biotechnology, China) to be reprobed with other antibodies. In this study, GAPDH or β-actin was used as the loading control. The relative level of each protein expression was normalized to GAPDH or β-actin. Values for target protein levels were calculated using Image J software (NIH, USA).

RNA extraction and quantitative real-time PCR

The mPFC were dissected immediately on ice. Total RNA was extracted from the mPFC using FastPure Cell/Tissue Total RNA Isolation Kit (Vazyme, China), according to the manufacturer's instructions. All samples were tested for concentration and purified using a 4200 TapeStation (Agilent Technologies, Santa Clara, USA). After RNA extraction, the amount of RNA was normalized across samples, and cDNA was created using HiScript II Q RT SuperMix for qPCR (+gDNA wiper) (Vazyme, China). *Gapdh* was used as the internal control. The primers used in the study were as follows:

Adrb1 (forward, CTCATCGTGGTGGGTAACGTG; reverse, ACACACAGCACATCTACCGAA). *c-Fos* (forward, CGGGTTTCAACGCCGACTA; reverse, TTGGCACTAGAGACGGACAGA). *Gapdh* (forward, AGGTCGGTGTGAACGGATTTG; reverse, TGTAGACCATGTAGTTGAGGTCA). The *Adrb1* and *c-Fos* mRNA levels were normalized to *Gapdh* mRNA levels. The relative mRNA level was calculated by the comparative CT method ($2^{-\Delta\Delta Ct}$).

Local administration of betaxolol in mPFC

The cannula-double (O.D. 0.30 mm, C.C 0.5, Mates with M 3.5, Cat 62121, RWD, China) were planted into mPFC (AP + 2.7 mm, ML ±0.3 mm, DV – 0.75 mm) of male F1 mice on PD63 before CPP training. After surgery, mice were maintained at home cage about 1 week. From PD70, F1 mice were subjected to METH-induced CPP training. In Experiment 1 (Figure 2a), a volume of 500 nL of betaxolol (specific antagonist for ADRB1) were bilaterally injected into mPFC at a rate of 100 nL/min at 15 min prior to CPP test on PD73. In Experiment 2 (Figure 2e), a volume of 500 nL of betaxolol bilaterally into the mPFC at a rate of 100 nL/min at 15 min prior to CPP training on PD71 and PD72.

Specific knockdown of ADRB1 on CaMKII-positive neurons in mPFC

On PD55, mice were anesthetized with 2% isoflurane in oxygen, and were fixed in a stereotactic frame (RWD, Shenzhen, China). A heating pad was used to maintain the core body temperature of the mice at 36 ℃. The coordinates of mPFC were defined as AP + 2.05 mm, ML ±0.3 mm, DV – 1.9 mm. A volume of 400 nL virus of *CaMKIIap-EGFP-MIR155 (MCS)-SV40PolyA* (KD group) (Titer, 2.41F + 13 v.g/mL; Cat, GIDV0286541, GeneChem, Shanghai, China) or *CaMKIIap-EGFP-SV40PolyA* (Ctrl group) (Titer, 4.01E + 12 v.g/mL; Cat, AAV9/CON540, GeneChem, Shanghai, China)

were injected bilaterally into mPFC at a rate of 80 nL/min. After surgery, mice were kept at homecage about 3 weeks.

Dendritic spine analysis

The dendritic spines of mPFC were photographed using the z-stack scanning function of Leica TCS SP8confocal microscope (Leica, Germany). The Spine quantification were performed under LAS X software (Leica, Germany). The number of spines is counting only in the second or the third branches of dendrites from the body of CaMKII-positive neurons. Density of spines were scored in about 50 μm dendritic segments in length.

Statistical analysis

Statistical analysis was carried out using GraphPad Prism 8.0.2 software. All data are presented as the Mean ± SD. CPP score are analyzed by two-way analysis of variance (ANOVA) with Sidak's multiple comparisons test, and other data are analyzed by unpaired *t*-tests. Statistical significance was set as $P < 0.05$.

Acknowledgment

This work is supported by National Natural Science Foundation of China (82071495), Natural Science Foundation of Jiangsu Province, China (BK20201398) and Natural Science Foundation of the Higher Education Institutions of Jiangsu Province, China (21KJB360007).

Author contribution

Zheng Y and Li Z have equal contribution to the manuscript. Zheng Y and Li Z performed behavioral tests, morphological tests. Wen J, Chen W, Guo H, Hu T, Zhang Y, Zhao Z and Cai Q assist the data analysis. Cheng Z carried out the virus-related

experiment. Ge F and Fan Y performed data analysis. Guan X and Fan Y wrote the manuscript. Guan X, Fan Y and Liu D developed the overall concept.

Conflict of interests

The authors have no conflict of interests to declare.

Data availability statement

The data that support the findings of this study are available from the corresponding author upon reasonable request.

Reference

1. Verstegen RHJ, et al. Paternal exposure to recreational drugs before conception and its effect on live-born offspring: A scoping review. *Birth defects research*. 2020;112(13):970-88.
2. Goldberg LR, and Gould TJ. Multigenerational and transgenerational effects of paternal exposure to drugs of abuse on behavioral and neural function. *The European journal of neuroscience.* 2019;50(3):2453-66.
3. Mihalčíková L, et al. Does paternal methamphetamine exposure affect the behavior of rat offspring during development and in adulthood? *Physiol Res.* 2021;70(S3):S419-S30.
4. Rushworth MF, et al. Frontal cortex and reward-guided learning and decision-making. *Neuron.* 2011;70(6):1054-69.
5. Horst N, and Laubach M. Reward-related activity in the medial prefrontal cortex is driven by consumption. *Frontiers in Neuroscience.* 2013;7(56.
6. Cordie R, and McFadden LM. Optogenetic inhibition of the medial prefrontal cortex reduces methamphetamine-primed reinstatement in male and female rats. *Behavioural pharmacology.* 2019;30(6):506-13.
7. Parsegian A, and See RE. Dysregulation of Dopamine and Glutamate Release in the Prefrontal Cortex and Nucleus Accumbens Following Methamphetamine Self-Administration and During Reinstatement in Rats. *Neuropsychopharmacology : official publication of the American College of Neuropsychopharmacology.* 2014;39(4):811-22.
8. Perry JL, et al. Prefrontal cortex and drug abuse vulnerability: translation to prevention and treatment interventions. *Brain Res Rev.* 2011;65(2):124-49.
9. Li H, et al. Behavioral sensitization induced by methamphetamine causes differential alterations

in gene expression and histone acetylation of the prefrontal cortex in rats. *BMC neuroscience.* 2021;22(1):24-.

10. Goldstein RZ, and Volkow ND. Dysfunction of the prefrontal cortex in addiction: neuroimaging findings and clinical implications. *Nature reviews Neuroscience.* 2011;12(11):652-69.

11. González B, et al. Repeated methamphetamine and modafinil induce differential cognitive effects and specific histone acetylation and DNA methylation profiles in the mouse medial prefrontal cortex. *Progress in neuro-psychopharmacology & biological psychiatry.* 2018;82(1-11.

12. Haddar M, et al. Inhibitory effects of Shati/Nat8l overexpression in the medial prefrontal cortex on methamphetamine-induced conditioned place preference in mice. *Addiction biology.* 2020;25(3):e12749.

13. Coutellier L, et al. β1-adrenergic receptor activation enhances memory in Alzheimer's disease model. *Ann Clin Transl Neurol.* 2014;1(5):348-60.

14. Goodman AM, et al. Heightened Hippocampal β-Adrenergic Receptor Function Drives Synaptic Potentiation and Supports Learning and Memory in the TgF344-AD Rat Model during Prodromal Alzheimer's Disease. *The Journal of neuroscience : the official journal of the Society for Neuroscience.* 2021;41(26):5747-61.

15. Rudoy CA, et al. Evidence for beta1-adrenergic receptor involvement in amygdalar corticotropin-releasing factor gene expression: implications for cocaine withdrawal. *Neuropsychopharmacology : official publication of the American College of Neuropsychopharmacology.* 2009;34(5):1135-48.

16. Sun Q, et al. Activation of β-adrenergic receptors during sexual arousal facilitates vaginal

lubrication by regulating vaginal epithelial Cl(-) secretion. *The journal of sexual medicine.* 2014;11(8):1936-48.

17. You Z-B, et al. Involvement of the ghrelin system in the maintenance and reinstatement of cocaine-motivated behaviors: a role of adrenergic action at peripheral β1 receptors. *Neuropsychopharmacology : official publication of the American College of Neuropsychopharmacology.* 2022;47(8):1449-60.

18. Sugama S, et al. Stress-induced microglial activation occurs through β-adrenergic receptor: noradrenaline as a key neurotransmitter in microglial activation. *Journal of neuroinflammation.* 2019;16(1):266.

19. Ji X-H, et al. Pre- and Postsynaptic β-Adrenergic Activation Enhances Excitatory Synaptic Transmission in Layer V/VI Pyramidal Neurons of the Medial Prefrontal Cortex of Rats. *Cerebral Cortex.* 2007;18(7):1506-20.

20. Vranjkovic O, et al. β-adrenergic receptor mediation of stress-induced reinstatement of extinguished cocaine-induced conditioned place preference in mice: roles for β1 and β2 adrenergic receptors. *The Journal of pharmacology and experimental therapeutics.* 2012;342(2):541-51.

21. Hernández A, et al. Effect of prenatal protein malnutrition on long-term potentiation and BDNF protein expression in the rat entorhinal cortex after neocortical and hippocampal tetanization. *Neural plasticity.* 2008;2008(646919.

22. Thompson BL, et al. Prenatal exposure to drugs: effects on brain development and implications for policy and education. *Nature reviews Neuroscience.* 2009;10(4):303-12.

23. Huang C-C, et al. Prenatal cocaine exposure enhances long-term potentiation induction in rat

medial prefrontal cortex. *International Journal of Neuropsychopharmacology.* 2011;14(4):431-43.

24. Meitzen J, et al. β1-Adrenergic receptors activate two distinct signaling pathways in striatal neurons. *Journal of neurochemistry.* 2011;116(6):984-95.

25. Huang B, et al. β-Arrestin-biased β-adrenergic signaling promotes extinction learning of cocaine reward memory. *Science Signaling.* 2018;11(512).

26. Goldberg LR, and Gould TJ. Multigenerational and transgenerational effects of paternal exposure to drugs of abuse on behavioral and neural function. *The European journal of neuroscience.* 2019;50(3):2453-66.

27. Vassoler FM, et al. The impact of exposure to addictive drugs on future generations: Physiological and behavioral effects. *Neuropharmacology.* 2014;76 Pt B(0 0):269-75.

28. Yaw AM, et al. Epigenetic effects of paternal cocaine on reward stimulus behavior and accumbens gene expression in mice. *Behav Brain Res.* 2019;367(68-81.

29. Maurer JJ, et al. Paternal nicotine taking elicits heritable sex-specific phenotypes that are mediated by hippocampal Satb2. *Molecular psychiatry.* 2022.

30. Lu H, et al. Cocaine exposure in utero alters synaptic plasticity in the medial prefrontal cortex of postnatal rats. *The Journal of neuroscience : the official journal of the Society for Neuroscience.* 2009;29(40):12664-74.

31. Morrow BA, et al. Prenatal exposure to cocaine is associated with increased number of spine synapses in rat prelimbic cortex. *Synapse.* 2007;61(10):862-5.

32. Crozatier C, et al. Altered cocaine-induced behavioral sensitization in adult mice exposed to cocaine in utero. *Brain research Developmental brain research.* 2003;147(1-2):97-105.

33. Yan QS, et al. Prenatal cocaine exposure decreases brain-derived neurotrophic factor proteins in the rat brain. *Brain research.* 2004;1009(1-2):228-33.

34. Cantacorps L, et al. Prenatal and postnatal alcohol exposure increases vulnerability to cocaine addiction in adult mice. *British journal of pharmacology.* 2020;177(5):1090-105.

35. Li Z, et al. Prenatal cocaine exposure alters functional activation in the ventral prefrontal cortex and its structural connectivity with the amygdala. *Psychiatry research.* 2013;213(1):47-55.

36. Rando K, et al. Prenatal cocaine exposure and gray matter volume in adolescent boys and girls: relationship to substance use initiation. *Biological psychiatry.* 2013;74(7):482-9.

37. Grewen K, et al. Prenatal cocaine effects on brain structure in early infancy. *NeuroImage.* 2014;101(114-23.

38. Yip SW, et al. Prenatal cocaine exposure, illicit-substance use and stress and craving processes during adolescence. *Drug and alcohol dependence.* 2016;158(76-85.

39. Grzelka K, et al. Noradrenaline Modulates the Membrane Potential and Holding Current of Medial Prefrontal Cortex Pyramidal Neurons via β(1)-Adrenergic Receptors and HCN Channels. *Front Cell Neurosci.* 2017;11(341-.

40. Henderson MG, et al. Long-term consequences of prenatal exposure to cocaine or related drugs: effects on rat brain monoaminergic receptors. *Brain research bulletin.* 1991;26(6):941-5.

41. Zhu H, et al. β1-Adrenoceptor in the Central Amygdala Is Required for Unconditioned Stimulus-Induced Drug Memory Reconsolidation. *The international journal of neuropsychopharmacology.* 2018;21(3):267-80.

42. Flores O, et al. Hidden prenatal malnutrition in the rat: role of β_1-adrenoceptors on synaptic plasticity in the frontal cortex. *Journal of neurochemistry.* 2011;119(2):314-23.

43. Liu X, et al. β-Arrestin-biased signaling mediates memory reconsolidation. *Proceedings of the National Academy of Sciences of the United States of America.* 2015;112(14):4483-8.

44. Son JS, et al. Regulatory Effect of Bee Venom on Methamphetamine-Induced Cellular Activities in Prefrontal Cortex and Nucleus Accumbens in Mice. *Biological and Pharmaceutical Bulletin.* 2015;38(1):48-52.

45. Sun WL, et al. Molecular Mechanism: ERK Signaling, Drug Addiction, and Behavioral Effects. *Progress in molecular biology and translational science.* 2016;137(1-40.

46. Lazenka MF, et al. Δ9-Tetrahydrocannabinol Experience Influences ΔFosB and Downstream Gene Expression in Prefrontal Cortex. *Cannabis and Cannabinoid Research.* 2017;2(1):224-34.

47. Ehrlich ME, et al. Periadolescent mice show enhanced DeltaFosB upregulation in response to cocaine and amphetamine. *The Journal of neuroscience : the official journal of the Society for Neuroscience.* 2002;22(21):9155-9.

48. Perrotti LI, et al. Distinct patterns of DeltaFosB induction in brain by drugs of abuse. *Synapse.* 2008;62(5):358-69.

49. Nestler EJ, et al. DeltaFosB: a sustained molecular switch for addiction. *Proceedings of the National Academy of Sciences of the United States of America.* 2001;98(20):11042-6.

Figure legends

Figure 1. METH-induced CPP behaviors, mPFC activities and ADRB1 levels in male F1 mice. a, Experimental design and timeline. **b**, CPP score. **c**, ΔCPP score. **d,** Traveled traces in CPP apparatus by F1 mice. **e-f**, The percentage of c-Fos-positive cells in Cg1, PrL and IL on PD60 and on PD73. CaMKII and c-Fos were used as markers for the pyramidal neurons and activated neurons, respectively. Scale bar, 500 μm /100 μm. **g-h**, Levels of c-Fos and CaMKII protein on PD60 and PD73. **i**, Levels of *Adrb1* mRNA on PD60 and PD73. **j**, Levels of ADRB1 protein on PD60 and PD73. **k-l**, Mean gray value of ADRB1 on mPFC neurons on PD60 and PD73. Scale bar, 500 μm /100 μm. Cg1, cingulate cortex; PrL, prelimbic cortex; IL, infralimbic cortex. SAL-sired mice, saline-sired male mice; METH-sired mice, methamphetamine-sired male mice. N.S., $P > 0.05$. $^{\#}$, $P < 0.05$ vs baseline (Pre-test CPP score). *, $P < 0.05$, **, $P < 0.01$ vs SAL-sired mice.

Figure 2. Local administration of betaxolol in mPFC and METH-induced CPP behaviors in METH-sired mice. a, Experimental design 1. **b**, CPP score of Experiment 1. **c**, ΔCPP score of Experiment 1. **d,** Traveled traces in the CPP apparatus by METH-sired mice of Experiment 1. **e**, Experimental design 2. **f**, CPP score of Experiment 2. **g**, ΔCPP score of Experiment 2. **h,** Traveled traces in the CPP apparatus by METH-sired mice of Experiment 2. F1-METH-Ts-Vcl, vehicle bilaterally into the mPFC of METH-sired mice at 15 min prior to CPP test; F1-METH-Ts-Bxol, betaxolol bilaterally into the mPFC of METH-sired mice at 15 min prior to CPP test; F1-METH-Tr-Vcl, vehicle bilaterally into the mPFC of METH-sired mice at 15 min prior to CPP training; F1-METH-Tr-Bxol, betaxolol bilaterally into the mPFC of METH-sired mice at 15 min prior to CPP training. N.S., $P > 0.05$. $^{\#\#}$, $P < 0.01$ vs baseline (Pre-test CPP score). **, $P < 0.01$ vs F1-METH-Ts-Vcl or F1-METH-Tr-Vcl.

Figure 3. Specific knockdown of ADRB1 on pyramidal neurons of mPFC and METH-induced CPP behaviors in METH-sired mice. a, Experimental design and timeline. **b**, Schematic diagram of viral injection and representative images of viral transfection in mPFC (middle pannel). Scale bar, 500 μm. **c**, Percentage of viral transfected neurons in the total pyramidal neurons of mPFC. Scale bar, 500 μm /100 μm. **d**, Levels of *Adrb1* mRNA in mPFC. **e**, Levels of ADRB1 protein in mPFC. **f**, Mean gray value of ADRB1 on virus transfected neurons of mPFC. Scale bar, 500 μm /100 μm. **g**, CPP score. **h**, .ΔCPP score. **i**, Traveled traces in the CPP apparatus by METH-sired mice. F1-METH-Ctrl, METH-sired mice injected with Ctrl virus. F1-METH-KD, METH-sired mice injected with KD virus. N.S., $P > 0.05$. $^{\#\#}$, $P < 0.01$ vs baseline (pre-test CPP score). *, $P < 0.05$, **, $P < 0.01$ vs F1-METH-Ctrl.

Figure 4. The mPFC activities, dendritic spine density and levels of downstream molecules of ADRB1 after ADRB1 knockdown. a, Levels of c-Fos and CaMKII protein. **b**, The c-Fos immunostaining. Scale bar, 500 μm /100 μm. **c**, Density of dendritic spine. Scale bar, 50 μm /10 μm. **d**, Levels of β-arestin2 and PKA protein. **e**, Levels of ERK1/2, p-ERK1/2, ERK1/2/p-ERK1/2, CREB, p-CREB, p-CREB/ CREB and ΔFosB protein. F1-METH-Ctrl, METH-sired mice injected with Ctrl virus. F1-METH-KD, METH-sired mice injected with KD virus. N.S., $P > 0.05$. *, $P < 0.05$, **, $P < 0.01$, vs F1-METH-Ctrl.

Figure 5. Graphical abstract. Paternal METH exposure decreased the baseline levels of c-Fos but increased that of ADRB1 in mPFC of F1 mice. Subthreshold dose of METH, which can not induce CPP and activate mPFC in naïve mice, could elicit significant METH-preferred behaviors in METH-sired mice, accompanied with higher levels of c-Fos immunostaining and ADRB1 in mPFC. Local blocking ADRB1 or specific knocking-down ADRB1 on excitatory neurons of mPFC efficiently inhibited

METH-induced CPP behaviors in METH-sired mice, and attenuated levels of c-Fos, p-ERK1/2, ΔFosB, dendritic spine density in their mPFC.

Supplementary Figure Legends

Figure S1. C-Fos expression and dendritic spine density of mPFC on PD73 of F1 mice. a, The number of c-Fos-positive neurons. Cg1, cingulate cortex; PrL, prelimbic cortex; IL, infralimbic cortex. Scale bar: 500 μm / 100 μm. **b,** Density of dendritic spine. Scale bar: 50 μm / 10 μm. SAL-sired mice, saline-sired male mice; METH-sired mice, methamphetamine-sired male mice. *, $P < 0.05$, **, $P < 0.01$, vs SAL-sired mice.

Figure S2. Effects of subthreshold-dosed administration of METH in naïve mice. a, Experimental design and timeline. **b**, Levels of *c-Fos* and *Adrb1* mRNA in mPFC. **c**, Levels of c-Fos and ADRB1 protein in mPFC. S, saline-injected mice. M, METH-injected mice. N.S., $P > 0.05$ vs S mice.

Figure S3. The schematic location of cannula in mPFC. a, Representative images of cannula location in mPFC.

Figure S4. Percentage of virus-transfected cells in mPFC. a, Percentage of EGFP-positive cells in total cells of mPFC. F1-METH-Ctrl, METH-sired mice injected with Ctrl virus. F1-METH-KD, METH-sired mice injected with KD virus. N.S., $P > 0.05$ vs F1-METH-Ctrl.

Figure 1

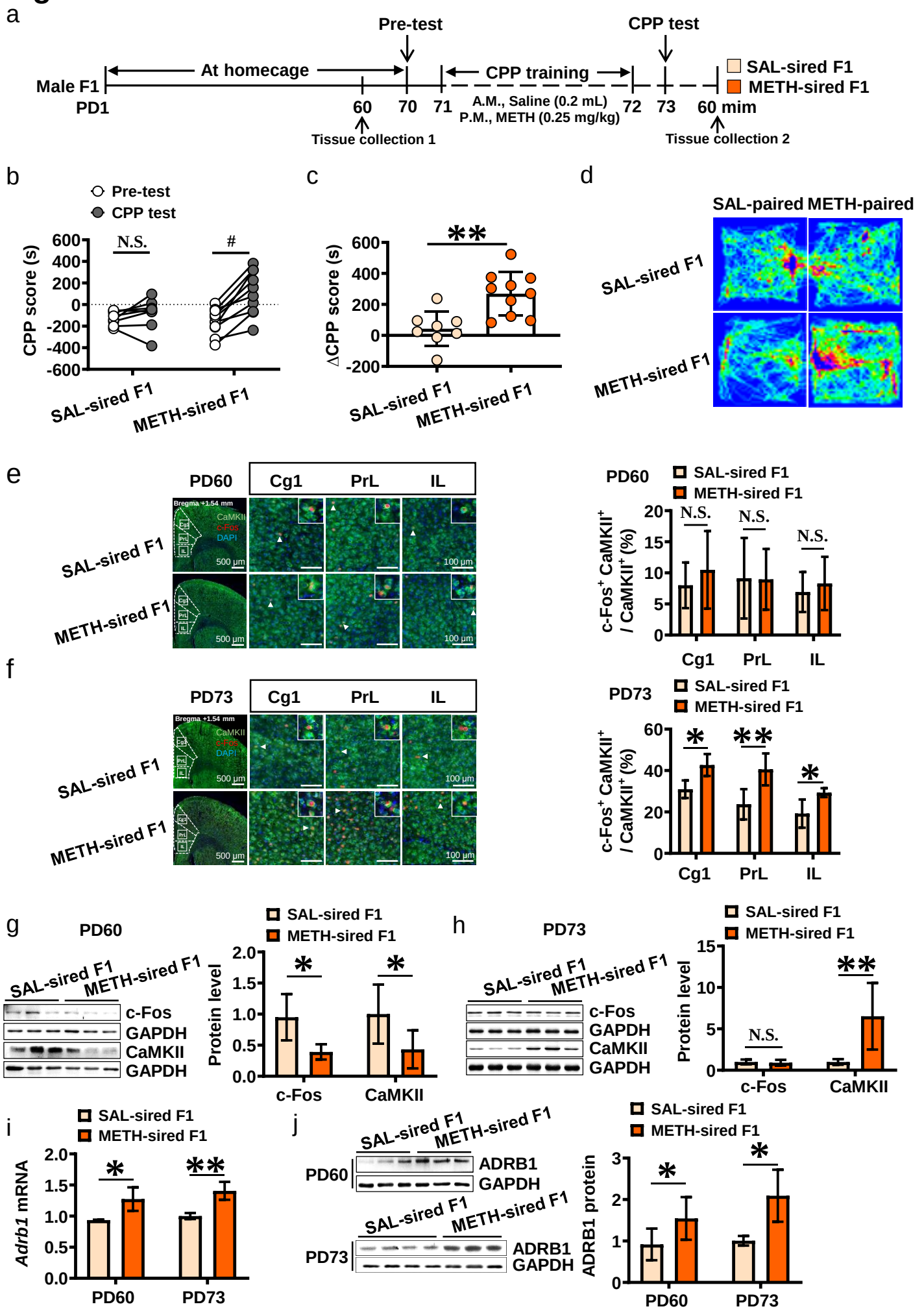
a
Pre-test
CPP test
Male F1
At homecage
CPP training
SAL-sired F1
METH-sired F1
PD1
60
70
71
A.M., Saline (0.2 mL)
P.M., METH (0.25 mg/kg)
72
73
60 mim
Tissue collection 1
Tissue collection 2
b
Pre-test
CPP test
CPP score (s)
N.S.
#
SAL-sired F1
METH-sired F1
c
ΔCPP score (s)
**
SAL-sired F1
METH-sired F1
d
SAL-paired
METH-paired
SAL-sired F1
METH-sired F1
e
PD60
Cg1
PrL
IL
Bregma +1.54 mm
CaMKII
c-Fos
DAPI
500 μm
100 μm
SAL-sired F1
METH-sired F1
PD60
SAL-sired F1
METH-sired F1
c-Fos+ CaMKII+ / CaMKII+ (%)
N.S.
N.S.
N.S.
Cg1
PrL
IL
f
PD73
Cg1
PrL
IL
SAL-sired F1
METH-sired F1
PD73
SAL-sired F1
METH-sired F1
c-Fos+ CaMKII+ / CaMKII+ (%)
*
**
*
Cg1
PrL
IL
g
PD60
SAL-sired F1
METH-sired F1
c-Fos
GAPDH
CaMKII
GAPDH
SAL-sired F1
METH-sired F1
Protein level
*
*
c-Fos
CaMKII
h
PD73
SAL-sired F1
METH-sired F1
c-Fos
GAPDH
CaMKII
GAPDH
SAL-sired F1
METH-sired F1
Protein level
N.S.
**
c-Fos
CaMKII
i
SAL-sired F1
METH-sired F1
Adrb1 mRNA
*
**
PD60
PD73
j
SAL-sired F1
METH-sired F1
PD60
ADRB1
GAPDH
SAL-sired F1
METH-sired F1
PD73
ADRB1
GAPDH
SAL-sired F1
METH-sired F1
ADRB1 protein
*
*
PD60
PD73

k

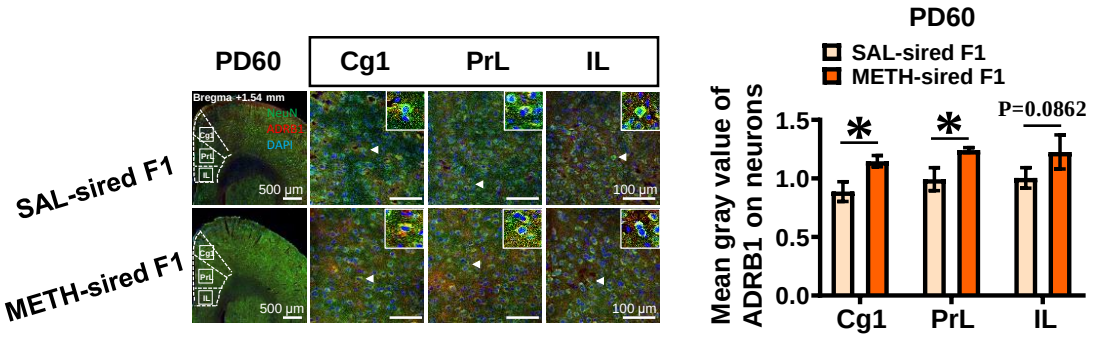
PD60
Cg1
PrL
IL
SAL-sired F1
METH-sired F1
Bregma +1.54 mm
NeuN
ADRB1
DAPI
500 µm
100 µm
PD60
SAL-sired F1
METH-sired F1
Mean gray value of ADRB1 on neurons
1.5
1.0
0.5
0.0
*
*
P=0.0862
Cg1
PrL
IL

l

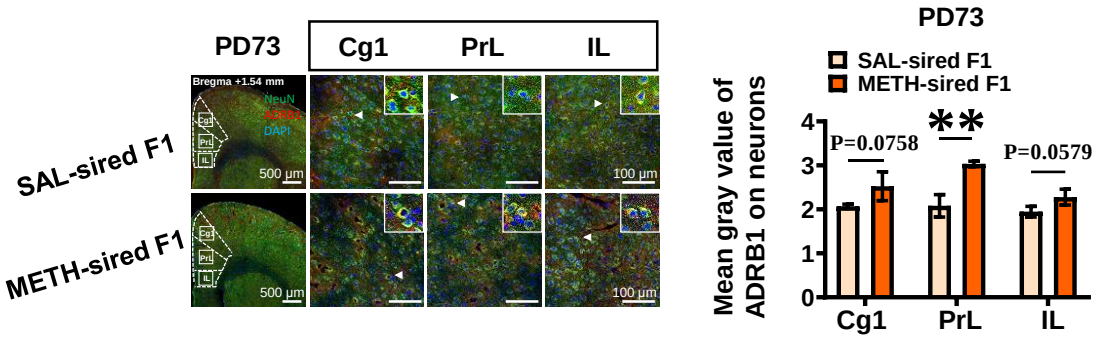
PD73
Cg1
PrL
IL
SAL-sired F1
METH-sired F1
Bregma +1.54 mm
NeuN
ADRB1
DAPI
500 µm
100 µm
PD73
SAL-sired F1
METH-sired F1
Mean gray value of ADRB1 on neurons
4
3
2
1
0
P=0.0758
**
P=0.0579
Cg1
PrL
IL

Figure 2

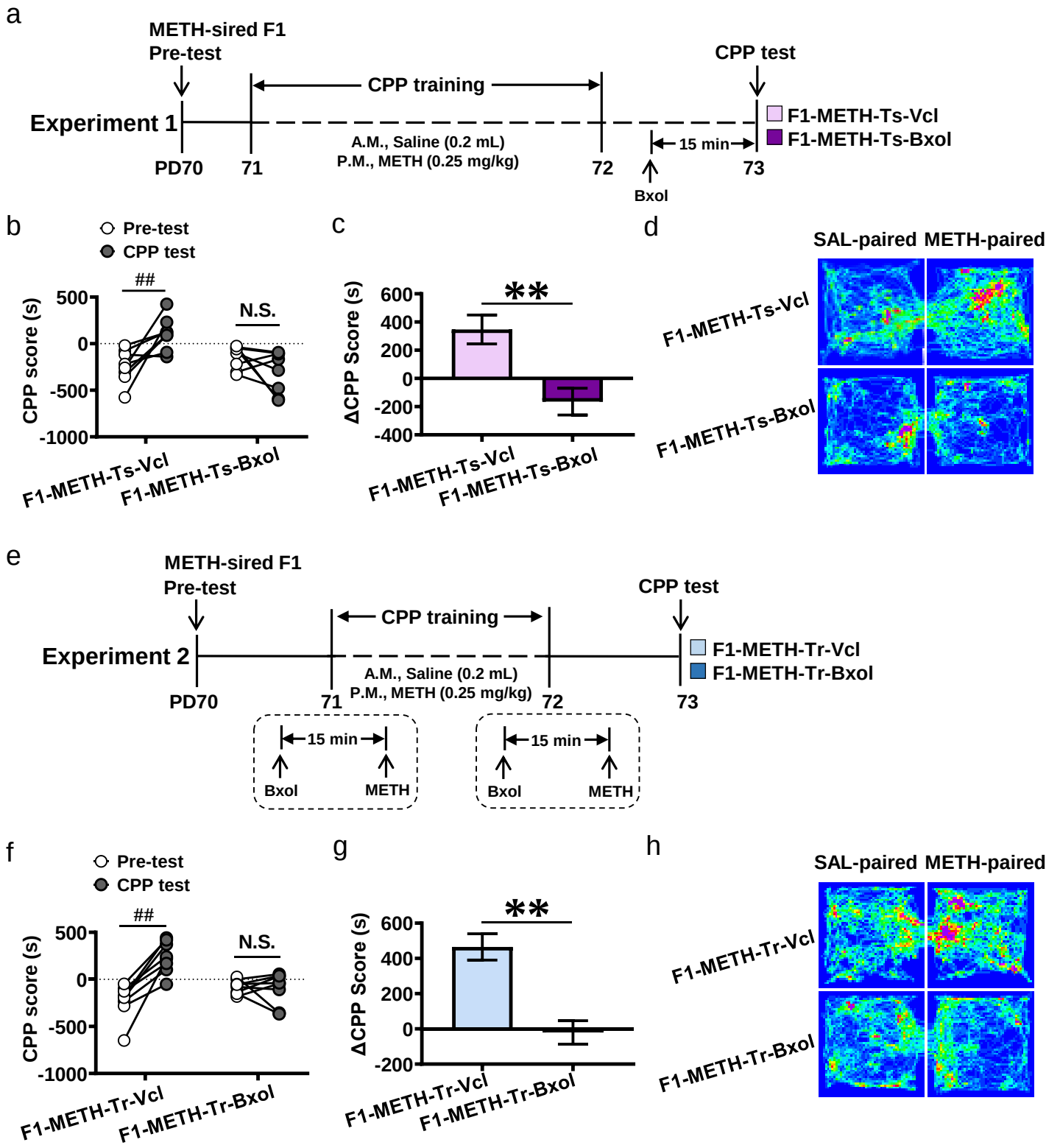
a
METH-sired F1
Pre-test
CPP test
CPP training
Experiment 1
F1-METH-Ts-Vcl
F1-METH-Ts-Bxol
A.M., Saline (0.2 mL)
P.M., METH (0.25 mg/kg)
15 min
PD70
71
72
73
Bxol
b
Pre-test
CPP test
##
N.S.
CPP score (s)
500
0
-500
-1000
F1-METH-Ts-Vcl
F1-METH-Ts-Bxol
c
**
ΔCPP Score (s)
600
400
200
0
-200
-400
F1-METH-Ts-Vcl
F1-METH-Ts-Bxol
d
SAL-paired
METH-paired
F1-METH-Ts-Vcl
F1-METH-Ts-Bxol
e
METH-sired F1
Pre-test
CPP test
CPP training
Experiment 2
F1-METH-Tr-Vcl
F1-METH-Tr-Bxol
A.M., Saline (0.2 mL)
P.M., METH (0.25 mg/kg)
PD70
71
72
73
15 min
Bxol
METH
15 min
Bxol
METH
f
Pre-test
CPP test
##
N.S.
CPP score (s)
500
0
-500
-1000
F1-METH-Tr-Vcl
F1-METH-Tr-Bxol
g
**
ΔCPP Score (s)
600
400
200
0
-200
F1-METH-Tr-Vcl
F1-METH-Tr-Bxol
h
SAL-paired
METH-paired
F1-METH-Tr-Vcl
F1-METH-Tr-Bxol

Figure 3

a

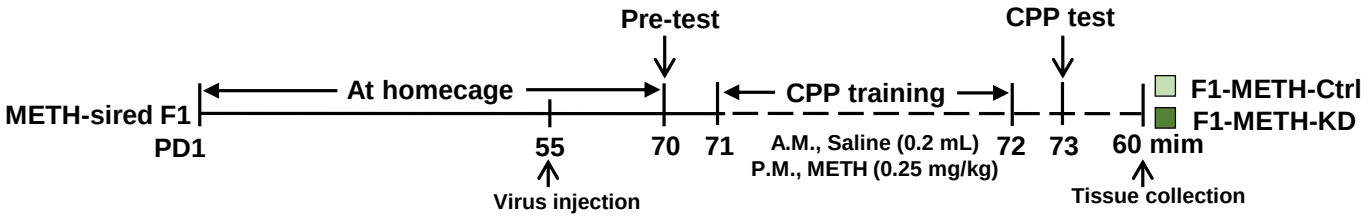

b

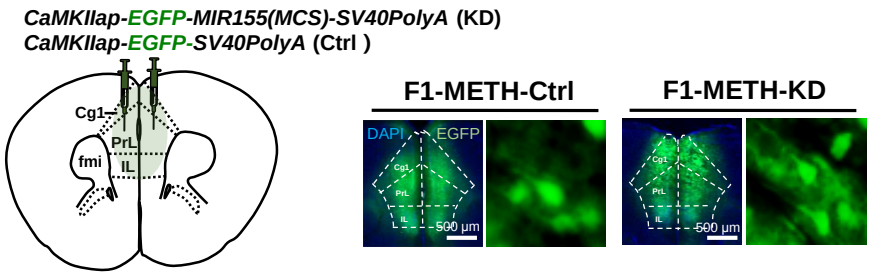

c

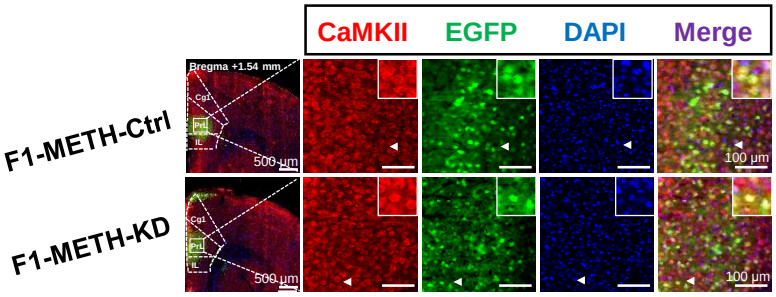

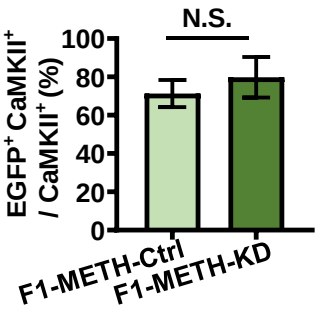

d

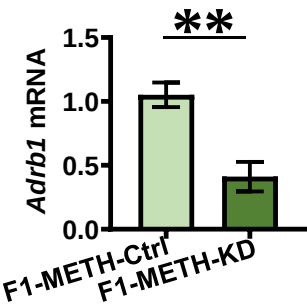

e

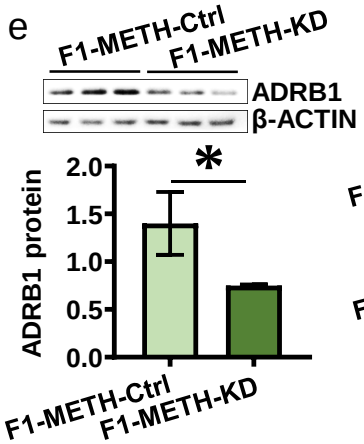

f

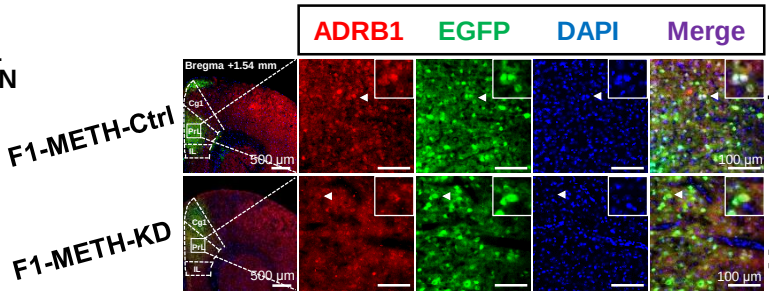

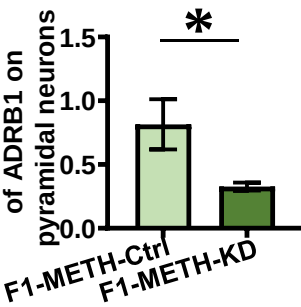

g

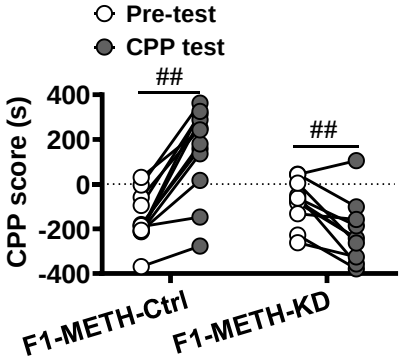

h

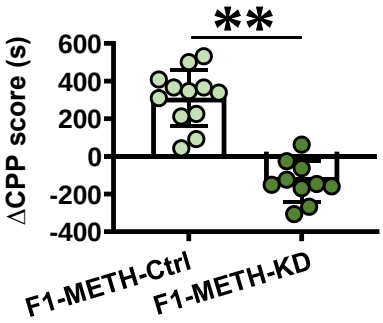

i

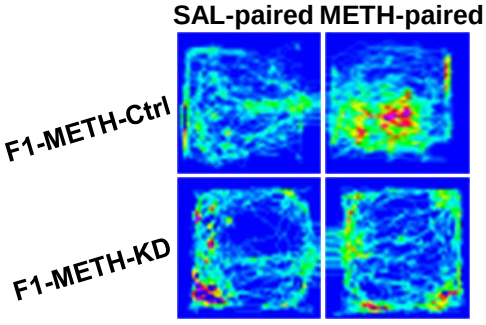

Figure 4

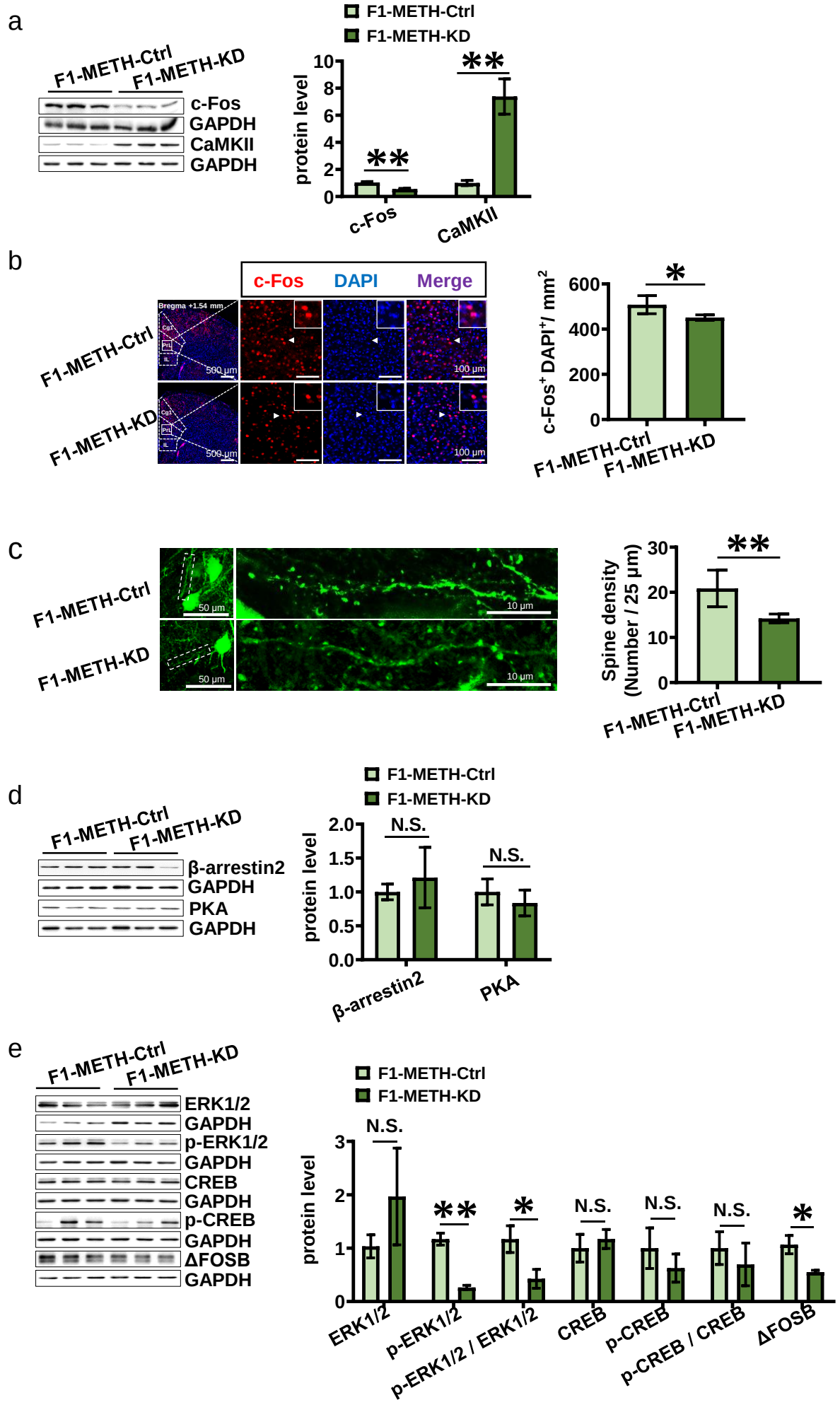
a
F1-METH-Ctrl
F1-METH-KD
c-Fos
GAPDH
CaMKII
GAPDH
protein level
c-Fos
CaMKII
b
c-Fos
DAPI
Merge
Bregma +1.54 mm
500 µm
100 µm
c-Fos+ DAPI+/ mm2
c
Spine density (Number / 25 µm)
50 µm
10 µm
d
β-arrestin2
PKA
N.S.
e
ERK1/2
p-ERK1/2
CREB
p-CREB
ΔFOSB
p-ERK1/2 / ERK1/2
p-CREB / CREB

Figure 5

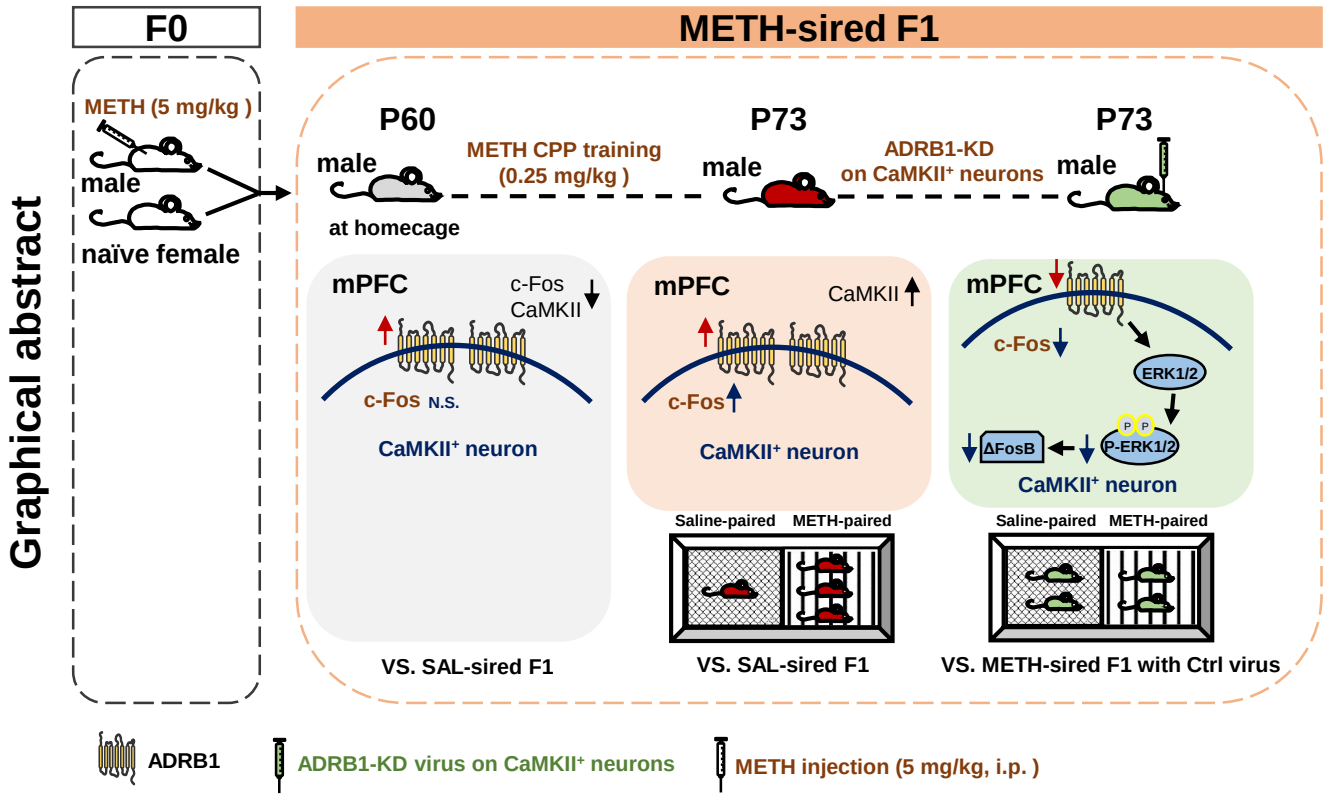
Graphical abstract
F0
METH (5 mg/kg)
male
naïve female
METH-sired F1
P60
male
at homecage
METH CPP training
(0.25 mg/kg)
P73
male
ADRB1-KD
on CaMKII+ neurons
P73
male
mPFC
c-Fos
CaMKII
c-Fos N.S.
CaMKII+ neuron
VS. SAL-sired F1
mPFC
CaMKII
c-Fos
CaMKII+ neuron
Saline-paired
METH-paired
VS. SAL-sired F1
mPFC
c-Fos
ERK1/2
ΔFosB
P-ERK1/2
CaMKII+ neuron
Saline-paired
METH-paired
VS. METH-sired F1 with Ctrl virus
ADRB1
ADRB1-KD virus on CaMKII+ neurons
METH injection (5 mg/kg, i.p.)

Figure S1

a

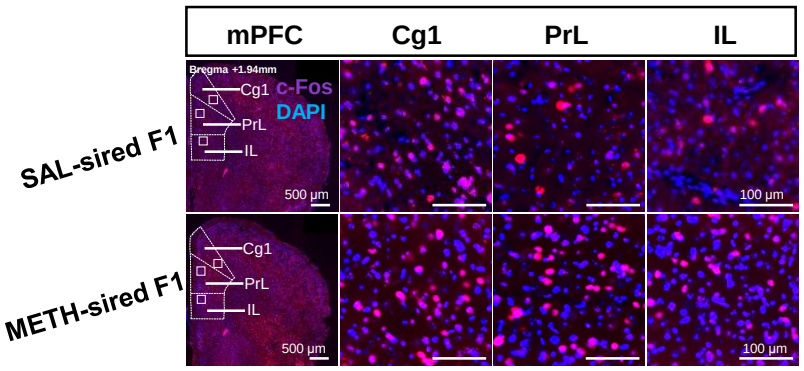
mPFC
Cg1
PrL
IL
SAL-sired F1
METH-sired F1
Bregma +1.94mm
Cg1
PrL
IL
c-Fos
DAPI
500 µm
100 µm

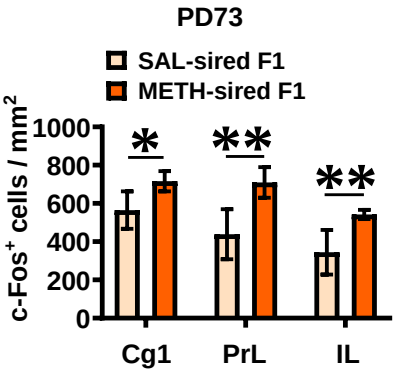
PD73
SAL-sired F1
METH-sired F1
c-Fos+ cells / mm2
1000
800
600
400
200
0
*
**
**
Cg1
PrL
IL

b

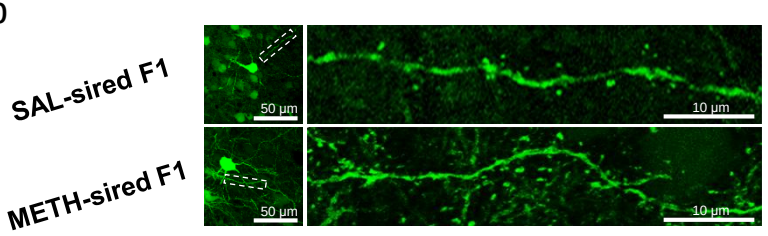
SAL-sired F1
METH-sired F1
50 µm
10 µm

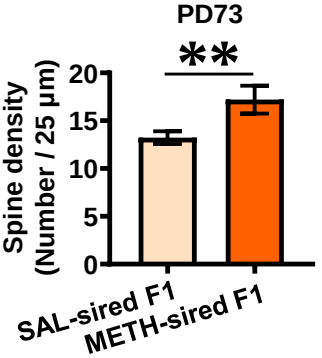
PD73
**
Spine density
(Number / 25 µm)
20
15
10
5
0
SAL-sired F1
METH-sired F1

Figure S2

a

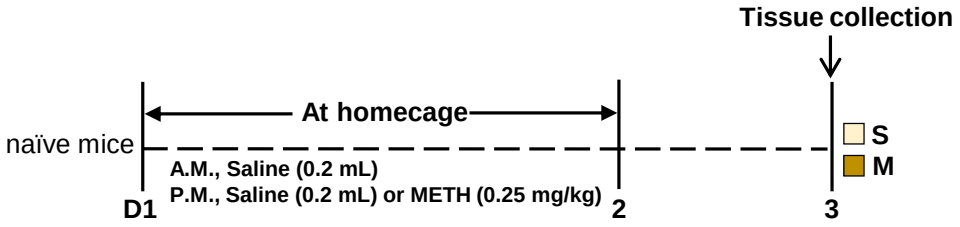

b

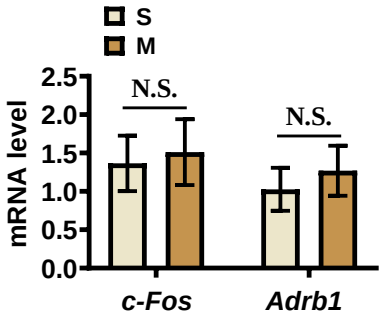

c

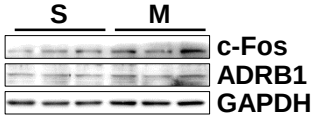

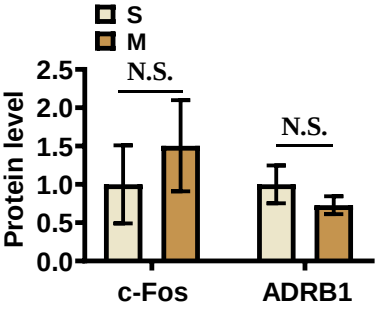

Figure S3

a

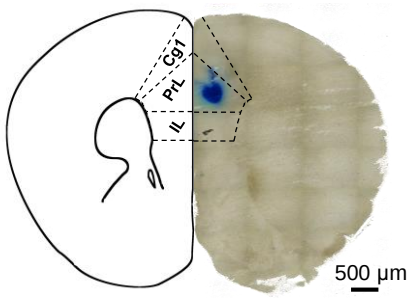

Bregma +1.94 mm

Figure S4
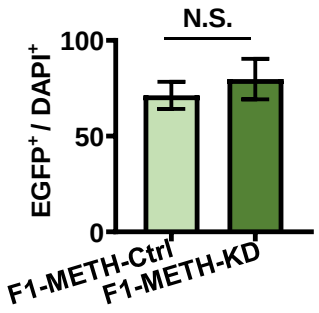
a